Front. Chem. Sci. Eng. 2025, 19(5): 37
https://doi.org/10.1007/s11705-025-2538-1

REVIEW ARTICLE

Controlled synthesis and advanced applications of ultralong carbon nanotubes

Fei Wang*, Yanlong Zhao*, Kangkang Wang, Khaixien Leu, Aike Xi, Qixuan Cai, Rufan Zhang (✉)

Beijing Key Laboratory of Green Chemical Reaction Engineering and Technology, Department of Chemical Engineering, Tsinghua University, Beijing 100084, China

Abstract Carbon nanotubes have attracted extensive interest owing to their extraordinary properties and wide applications in many fields. Among various types of carbon nanotubes, only ultralong carbon nanotubes with macroscale lengths, low defect concentrations, and high degrees of alignment can fully demonstrate their intrinsic performance. These attributes make ultralong carbon nanotubes highly promising for applications in cutting-edge fields, such as carbon-based integrated circuits, ultra-strong fibers, and transparent conductive films. However, the mass production of ultralong carbon nanotubes with precise structural control remains a major challenge, limiting their widespread applications. In the past decades, great progress has been achieved in the study of ultralong carbon nanotubes. In this review, we summarized the growth mechanisms and the controlled synthesis strategies of ultralong carbon nanotubes. Then, we introduced the advanced applications of ultralong carbon nanotubes in many areas, such as field-effect transistors, sensors, and photodetectors. Finally, we discussed the remaining challenges and offered our perspectives on the future directions of this field.

Keywords carbon nanotubes, ultralong, controlled synthesis, advanced application

1 Introduction

Since their discovery by Iijima in 1991, carbon nanotubes (CNTs) have attracted extensive attention from both the academic and industrial communities worldwide [1]. The structure of a CNT can be regarded as rolling up a graphene nanosheet along a specific vector into a tube, and this unique atomic structure endows them with outstanding mechanical, electrical, optical, and thermal properties [2]. For instance, CNTs theoretically possess an exceptionally high Young's modulus of up to 1 TPa and a tensile strength reaching 100 GPa [3]. Their weight-specific strength is at least four hundred times higher than that of steel [4]. Besides, their thermal and electrical conductivities are as high as 3500 $W \cdot m^{-1} \cdot K^{-1}$ and 2×10^7 $S \cdot m^{-1}$, respectively [5]. Additionally, the unique band structure of CNTs enables them to achieve ultra-broadband absorption of electromagnetic waves across the ultraviolet to terahertz spectrum, enabling functionalities such as photodetection, photoluminescence, electroluminescence, and electromagnetic shielding [6−8]. Given the excellent properties of CNTs, they have broad application prospects in fields such as ultra-strong fibers, carbon-based integrated circuits, mechanical energy storage, and flexible electronic devices [9−12].

After decades of development, the mass production of CNTs has been achieved, and they are widely applied in conductive additives, high-strength fibers, polymer composites, electrochemical energy storage, and so on [13−15]. However, the structural defect and short length (< 100 μm) in the mass-produced CNTs make their properties much lower than theoretical predictions. Therefore, it is important to prepare CNTs with perfect structures and macroscopic lengths, which can fully exhibit their intrinsic excellent properties. Generally, CNTs can be classified into three types based on morphological differences: agglomerated CNTs, vertically aligned CNT arrays (VACNT), and horizontally aligned CNT arrays (HACNT) [2]. However, the agglomerated CNTs and VACNTs usually suffer from short lengths and many structure defects resulting in significantly lower performance than theoretical values [16,17]. The HACNTs are usually grown on flat substrates, exhibiting very low defect concentrations and excellent properties. There are two types of HACNTs that follow the base-

Received December 1, 2024; accepted January 13, 2025;
online March 25, 2025

E-mail: zhangrufan@tsinghua.edu.cn

*These authors contributed equally to this work.

growth mode and tip-growth mode, respectively. The base-growth HACNTs usually have strong interactions with substrates, resulting in a slow growth rate and short lengths (< 1 mm). Conversely, the tip-growth HACNTs float in the gas flow during their growth, which prevents interference and resistance from the substrates. As a result, these CNTs exhibit very rapid growth rates, with lengths reaching several centimeters or even decimeters. Consequently, these tip-growth CNTs are often referred to as "ultralong CNTs". In conclusion, among all types of CNTs, only ultralong CNTs with macroscale lengths, low defect concentrations, and high degrees of alignment can fully demonstrate their intrinsic performance, and meet the strict requirements of cutting-edge fields.

However, the mass production of ultralong CNTs remains a significant challenge that severely hinders their practical application. Currently, the array density of ultralong CNTs is typically less than 100 tubes·mm^{-1}, which is far below the target of 125000 tubes·mm^{-1} proposed by the International Business Machines Corporation for carbon-based integrated circuits [18]. Furthermore, this low yield is insufficient to support the large-scale fabrication of macroscopic CNT films, fibers, and other assemblies. Over the past three decades, researchers have conducted extensive investigations into various aspects of ultralong CNTs, including their growth mechanisms, property studies, synthesis strategies, and applications. Herein, we discussed the growth mechanisms of ultralong CNTs to reveal the reasons for their low array density and reviewed the recent advancements in the controlled synthesis of high-density ultralong CNTs and their advanced applications. We hope this review will provide insights into the future prospects for the mass production of ultralong CNTs and their applications.

2 Growth mechanism of ultralong CNTs

The refinement of CNT fabrication techniques is fundamental to realizing the practical applications of CNTs. CNTs can be synthesized via a variety of techniques, among which chemical vapor deposition (CVD) [19], arc discharge [1,20], and laser ablation [21,22] are recognized as the predominant methods in this field. Both arc discharge and laser ablation methods produce CNTs with fewer metal impurities and amorphous carbon compared with other techniques. However, the arc discharge method requires more complex equipment and often results in CNT agglomeration, leading to structural defects. Furthermore, CNTs produced via this method can fuse with other byproducts and nanoparticles, complicating the subsequent separation and purification processes. Although laser ablation is effective in producing high-purity CNTs, its limitations in equipment scalability make it unsuitable for large-scale production. In contrast, CVD offers unique advantages in the fine control of CNT structure, orientation-controlled growth, macro-scale morphology regulation, and large-scale production. CVD is currently the most promising technique for mass production, as it allows for precise control over CNT structure and properties, positioning it as the leading method for the scalable production of high-quality CNTs.

2.1 Base-growth and tip-growth mechanisms

CNT growth is generally based on the "solution-precipitation" model [23]. First, carbon atoms generated from the decomposition of carbon sources contact with the exposed catalyst surface and dissolve into the catalyst. The formation of CNTs begins with nucleation, where carbon atoms adsorb onto the substrate and aggregate through surface diffusion to form a ring-like structure. This structure then evolves into a tube, marking the initial stage of CNT growth. The dissolved carbon atoms are transported to other sites on the catalyst, where they precipitate and are deposited onto the tube walls in a specific orientation. This process is essential for the continuous elongation of the CNT, with carbon atoms adding layer by layer to form the final structure. In the CVD process, carbon-containing gases, including methane and acetylene, are introduced into a reactor operating at elevated temperatures. Then, the gases decompose, leading to the deposition of carbon onto catalyst particles. This process involves two primary growth modes: base-growth and tip-growth (Fig. 1(a)).

In the base-growth mechanism, the catalyst is anchored to the substrate. As the newly formed CNT grows, its tip gradually moves away from the catalyst, causing the catalyst to remain at the base of the CNT. It is fundamentally attributed to the strong interaction between the catalyst and the substrate, which restricts the detachment of the catalyst from the substrate. Yoshida et al. [25] employed *in situ* transmission electron microscopy (TEM) to observe the growth behavior of CNTs at 600 °C (Fig. 1(b)). Their observations revealed that the catalysts and support were in close contact, with CNTs nucleating and growing directly on the catalyst surfaces. As the CNTs grew, their tips gradually moved away from the catalyst, extending outwards. He et al. [26] demonstrated that CNTs grown on SiO_2/Si substrates followed a base-growth mode by regenerating the catalyst through air calcination. This catalytic regeneration was essential for maintaining the growth of CNTs in a consistent, as the catalytic particles reformed and re-activated at the interface between the catalyst and the growing nanotube (Fig. 1(c)).

The base-growth mode is more conducive to controlling the structure of CNTs, primarily due to the lower growth temperatures typically used and the strong interactions between the substrate and the catalyst. These

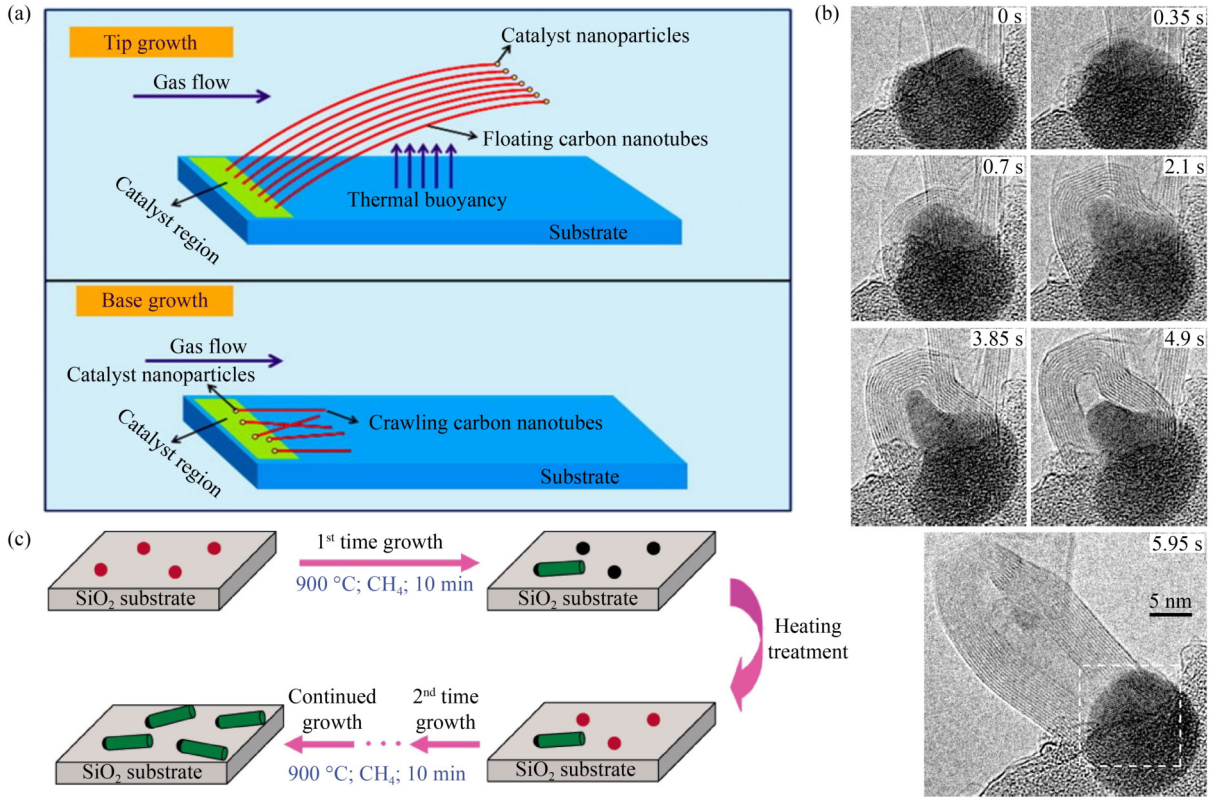

Fig. 1 (a) The scheme of tip-growth mechanism and base growth mechanism for CNTs. Reprinted with permission from Ref. [24], copyright 2013, Elsevier. (b) Nucleation and growth of multi-walled CNTs from a nanoparticle catalyst on a substrate. The growth recording time is shown in the images. Reprinted with permission from Ref. [25], copyright 2008, American Chemical Society. (c) Schematic illustration of multi-time growth of single-walled CNTs on SiO_2 substrates, with catalyst regeneration in heating air. Reprinted with permission from Ref. [26], copyright 2004, American Chemical Society.

factors restrict catalyst movement at high temperatures, enabling it to maintain a relatively stable morphology. The slower growth rate in base-growth mode promotes the templated growth of CNTs, with the catalyst acting as a template during both nucleation and growth stages. However, the catalyst particles remain fixed on the substrate throughout the process. As a result, their catalytic activity is more susceptible to interference from the substrate, and the mass transport resistance at the catalyst surface is greater compared to catalyst particles suspended in a flow of gas. This leads to an increased likelihood of defects and it also promotes the growth of shorter nanotubes during the growth process.

In the tip-growth mode, the catalyst becomes detached from the substrate or support and is positioned at the tip of the growing CNT. Under the supply of carbon sources, the catalyst drives the growth of the nanotube, with its spatial position constantly changing. The fundamental reason for tip-growth lies in the relatively weak interaction between the catalyst and the substrate. As carbon atoms assemble on the catalyst surface, this process induces the separation of the catalyst from the substrate. Helveg et al. [27] used *in situ* TEM to observe the real-time growth of CNTs. They found that at 536 °C with a 1:1 ratio of CH_4 to H_2 as the gas feed, CNTs grew via the tip-growth mode when Ni was used as the catalyst (Fig. 2(a)). Additionally, the tip-growth mode of ultralong CNTs has also been confirmed using isotopic labeling techniques. In this approach, Raman spectroscopy was employed to distinguish between ^{12}C and ^{13}C [28], with ^{13}C chosen as the marker for CNT growth (Fig. 2(b)). During the synthesis of HACNTs, growth was first carried out under a $^{12}CH_4$ atmosphere for a period, followed by a switch to $^{13}CH_4$. Raman spectroscopy revealed that ^{12}C was located at the initial end of the nanotube, near the catalyst region, while ^{13}C was found at the tip, far from the original catalyst loading. This result provides direct evidence that HACNTs grown on SiO_2/Si substrates follow the tip-growth mode.

The tip-growth mode is more conducive to producing structurally perfect CNTs, as it allows the nanotubes to float within the gas flow, minimizing interference from the substrate and reducing the likelihood of defects. Additionally, tip-growth is more suitable for the selective growth of ultralong CNTs, as the higher growth rates and large macroscopic lengths of these nanotubes require a significant number of carbon source molecules to decompose on the catalyst surface in the gas phase. Catalysts suspended within the gas flow are clearly better positioned to meet this requirement.

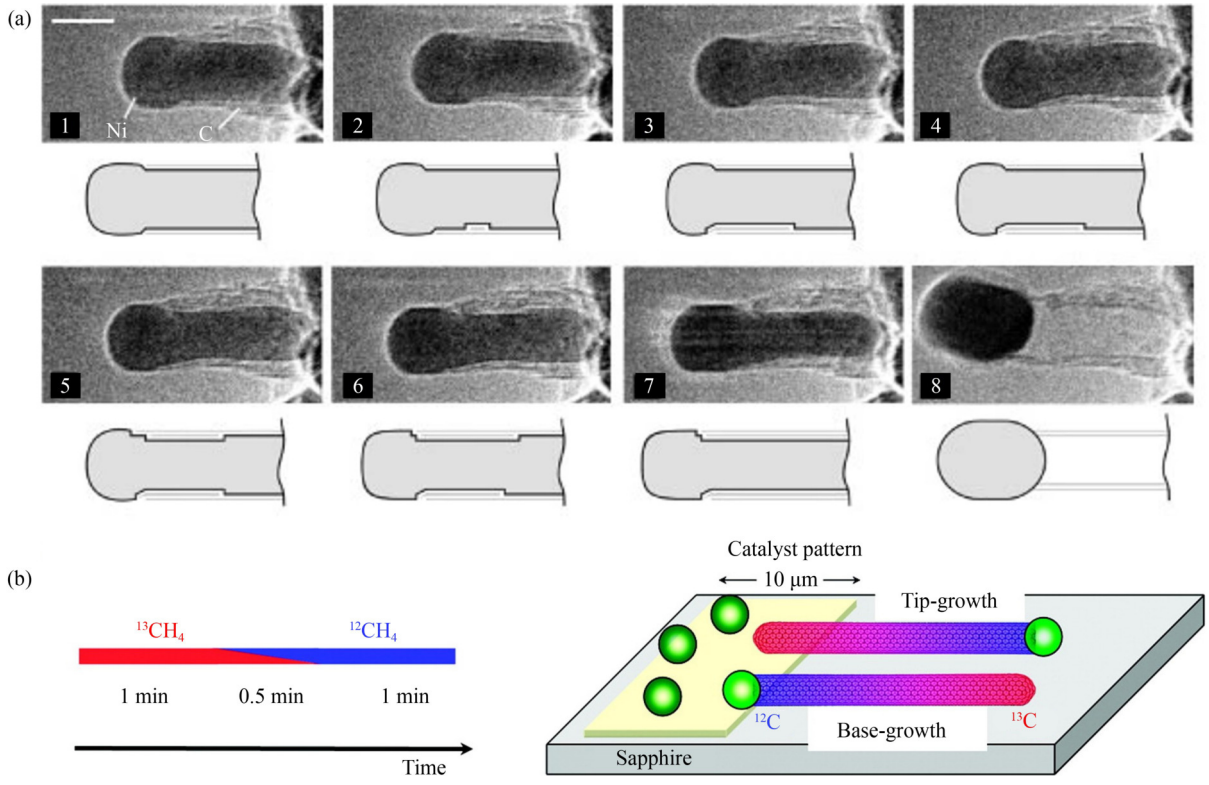

Fig. 2 (a) Image sequence of a growing CNT. Drawings are included to guide the eye in locating the positions of mono-atomic Ni step edges at the C–Ni interface. Reprinted with permission from Ref. [27], copyright 2004, Springer Nature. (b) Timing of the carbon feedstock supply for $^{13}C/^{12}C$-labeled single-walled CNTs growth and the resulting nanotubes expected for the base- and tip-growth modes. Reprinted with permission from Ref. [28], copyright 2008, American Chemical Society.

2.2 Growth mechanism of ultralong CNTs

The growth of ultralong CNTs follows a tip-growth mechanism. In this process, the catalyst is positioned at the tip of the nanotube, suspended in the gas flow, where it catalyzes the elongation of the nanotube along the flow direction [29]. Because the catalyst remains in a free-floating state during growth, this mechanism favors the formation of CNTs with both exceptional lengths and high structural integrity. This mode allows for the free growth of CNTs, facilitating the formation of horizontal arrays with macroscopic lengths and perfect structures.

During the growth of ultralong CNTs, a temperature difference between the substrate and the airflow creates a "thermal buoyancy" effect above the substrate. CNTs begin to grow from one end of the flat substrate, and their tips gradually detach from the catalyst under the combined influence of airflow drag, thermal buoyancy, and the van der Waals forces from the substrate. This detachment causes the CNTs to float in the gas phase, resembling a kite. This "kite growth" mode minimizes wall effects during the growth process, as the CNTs are no longer constrained by the substrate (Fig. 3(a)). As a result, ultralong CNTs exhibit rapid growth rates and perfect structural integrity. Therefore, the floating state is a key feature of ultralong CNT growth, although the underlying mechanism for this floating behavior remains unclear. Zhang et al. [30] proposed a simple and quantitative thermal balance model to describe the inherent thermal effects of the substrate, which can explain the temperature difference between the substrate and the surrounding airflow (Fig. 3(b)). Based on this thermal balance model, the authors derived a positive correlation between the substrate temperature and its emissivity, and they used this relationship to analyze the influence of substrate emissivity on the growth of ultralong CNTs. By leveraging inherent thermal effects of the substrates and thermophoresis, they achieved localized temperature control within the reactor, which allowed them to manipulate the density and orientation of ultralong CNT arrays.

Further investigations revealed the presence of catalyst particles at the tip of the CNT, validating the tip-growth mechanism for gas flow-induced alignment of CNTs. Additionally, experiments demonstrated that CNT arrays could grow across trenches up to several micrometers or even millimeters deep (Fig. 3(c)), or grow over obstacles as high as tens of micrometers [31,33,34]. *In situ* rotation of the substrate during growth resulted in changes to the alignment of the CNT arrays (Fig. 3(d)), providing further evidence that these arrays grow in a directionally controlled manner within the gas flow [32].

The growth of CNTs follows a mechanism analogous to polymer chain reactions, and their growth kinetics can be

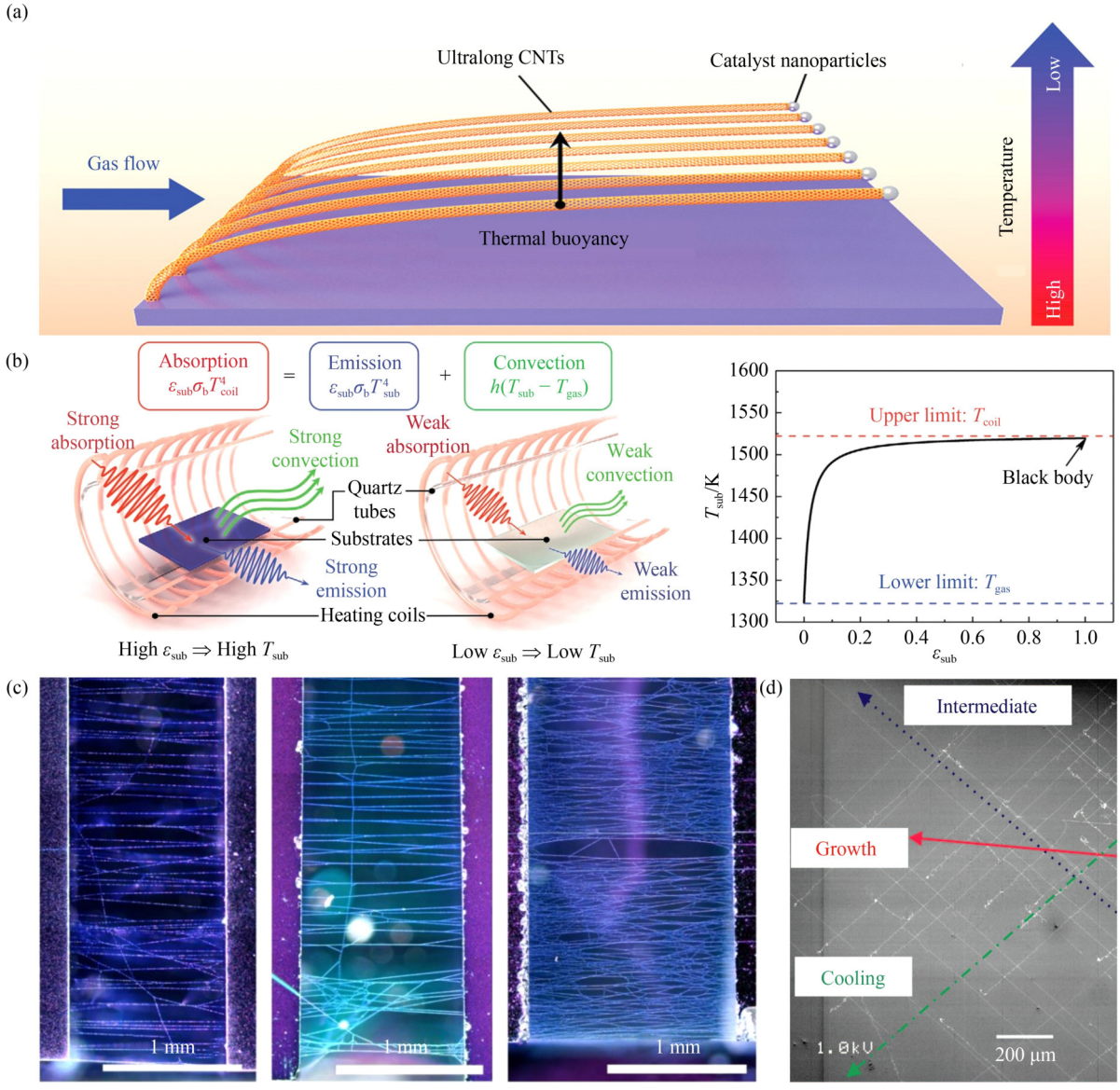

Fig. 3 (a) Schematic illustration of the flying kite-like growth mechanism of ultralong CNTs. (b) Schematic illustration of the heat balance of the substrates with different emissivity and relationship between substrate temperature and substrate emissivity. Reprinted with permission from Ref. [30], copyright 2022, Wiley-VCH. (c) Optical visualization of suspended CNT networks across the trench. Reprinted with permission from Ref. [31], copyright 2022, Wiley-VCH. (d) Scanning electron microscopy (SEM) image of the resulting aligned nanotubes with an indication of the gas flow direction for each of the corresponding phases. Reprinted with permission from Ref. [32], copyright 2008, American Chemical Society.

analyzed using principles derived from polymer chain elongation theory. By applying the Schulz-Flory distribution [35], a model developed in polymer science, it is possible to explain the length distribution of CNTs during the alignment process. In most cases, the supply of carbon sources is adequate to sustain CNT growth. Key parameters, such as temperature, gas flow rate, carbon source type, and gas composition, influence growth primarily by modulating the catalytic activity of the catalyst. Consequently, the maintenance of catalytic activity during nanotube elongation is a probabilistic event [36]. Under steady-state conditions (Fig. 4(a)), with all other factors held constant, the probability of maintaining catalyst activity is denoted as α, while the probability of catalyst deactivation is $1 - \alpha$. Thus, the proportion of CNTs with length l in the fabricated horizontal array can be expressed as:

$$P_l = \alpha^{l-1}(1-\alpha).$$

The equation above clearly demonstrates that as α decreases, the proportion of shorter nanotubes increases. Moreover, the density of CNTs follows an exponential decay with increasing length, which provides a coherent explanation for the experimentally observed sharp reduction in CNT density along the length direction in horizontal arrays. Based on this analysis, a practical

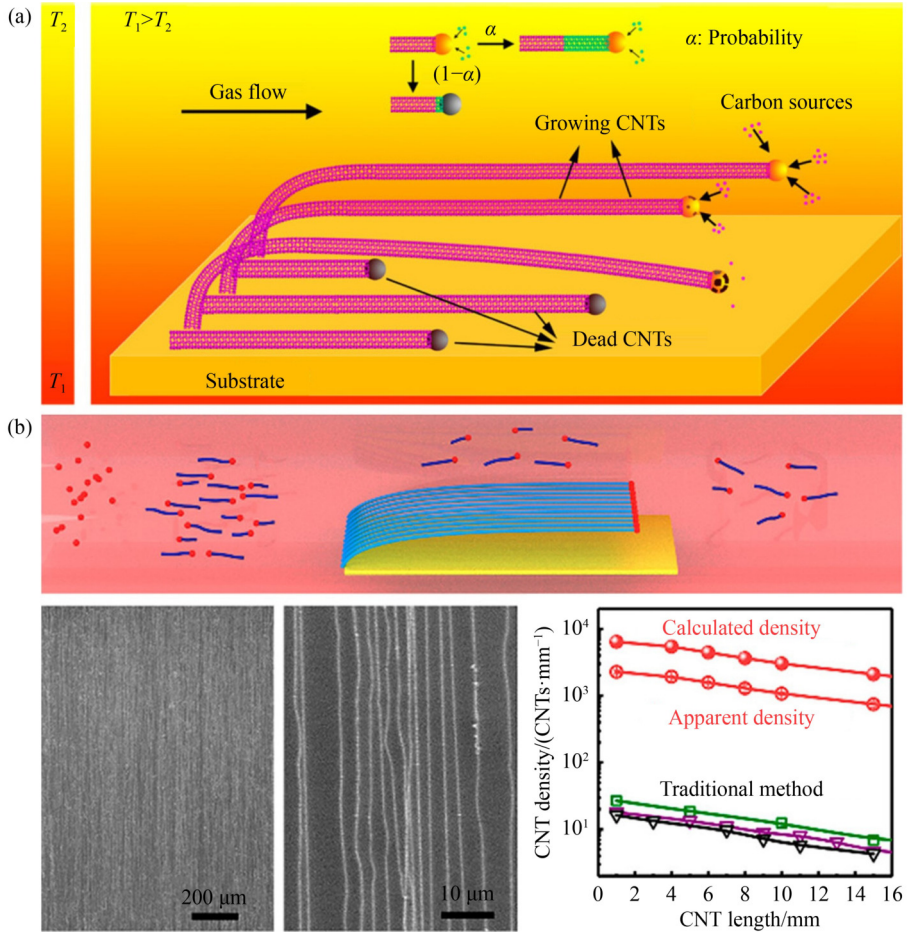

Fig. 4 (a) Growth of ultralong CNTs and illustration of tip-growth of ultralong CNTs. Reprinted with permission from Ref. [36], copyright 2013, American Chemical Society. (b) Schematic of the experimental setup and growth process of ultralong CNT arrays by SIDS. SEM images of the high-density ultralong CNT arrays, and comparison of the areal densities of ultralong CNT arrays synthesized by SIDS and traditional methods. Reprinted with permission from Ref. [37], copyright 2023, American Chemical Society.

strategy to increase the proportion of ultralong CNTs in the horizontal array CNTs, while ensuring sufficient carbon source availability, is to optimize the catalytic activity of the catalyst.

According to the kite mechanism model, Jiang et al. [37] explored the intrinsic relationship between the growth mechanisms of CNTs and ultralong CNTs synthesized via the floating catalyst CVD (FCCVD) method. They proposed a novel strategy, known as the substrate interception and direction strategy (SIDS), to achieve ultra-high-yield production of ultralong CNTs. SIDS enables the transition of floating short CNTs grown by FCCVD into the growth mode of ultralong CNTs. This approach significantly enhances catalyst utilization, reduces the tendency for coalescence, and increases the array density of ultralong CNTs to approximately 6700 tubes·mm^{-1}, at least two orders of magnitude higher than conventional methods (Fig. 4(b)). Furthermore, CNTs produced via SIDS exhibit remarkable properties, including decimeter-scale length, near-perfect structure, and high semiconductor purity. The versatility of the SIDS method is demonstrated across various substrates, such as silicon wafers, quartz, and quartz glass, and can be applied to construct well-ordered interwoven networks of ultralong CNTs.

3 Structural control of ultralong CNTs

The structural control of ultralong CNTs is crucial for optimizing their properties for various applications. Key parameters influencing their structure include length, areal density, wall number, diameter, and overall morphology. Length can be controlled through adjustments in synthesis conditions, such as reaction time and catalyst activity, while areal density can be optimized by manipulating catalyst distribution and deposition methods. The wall number and diameter of CNTs are influenced by catalyst size and synthesis parameters, with smaller catalysts typically yielding single-walled structures. Additionally, controlling morphology through substrate selection and synthesis conditions enhances the

alignment and curvature of CNTs, thereby improving their performance in applications ranging from nanoelectronics to composites. Overall, precise structural control is essential for developing high-quality ultralong CNTs tailored for specific technological advancements.

3.1 Control of the length of ultralong CNTs

The gas flow-induced method, in addition to the substrate-induced method, represents a key approach for the fabrication of HACNTs. In CVD, the gas flow directs the CNTs to float and grow along the flow direction, resulting in parallel, macroscopically long, and structurally perfect CNT arrays. This floating growth minimizes environmental interference and constraints, leading to fewer defects. Moreover, CNTs grown by this method can achieve lengths ranging from centimeters to meters, which enhances the manifestation of their intrinsic properties, such as exceptional mechanical strength and outstanding electrical conductivity.

The growth of CNTs requires a high-temperature environment to facilitate both the pyrolysis of the carbon source and the catalytic growth of the nanotubes. However, when the temperature exceeds the optimal range for CNT growth, the catalytic activity increases, leading to accelerated cracking of the carbon source. This results in the excessive decomposition of carbon, which can deposit as amorphous carbon on the catalyst surface, thereby reducing its catalytic activity. To address this challenge, Zhang et al. [36] developed a "moving isothermal zone" method for the synthesis of ultralong CNTs (Fig. 5(a)). This approach effectively extends the isothermal zone within the tube furnace by using a motor to drive the furnace body, allowing it to move along the growth direction of the CNTs at a rate corresponding to the nanotube growth rate. This movement increases the effective growth time of the CNTs and enables the production of nanotubes with lengths on the meter scale (Fig. 5(b)).

Despite of temperature, several other factors are critical for enhancing catalyst activity, including the type of carbon source, gas composition, catalyst material, particle size, and substrate type. The catalysts commonly used for the growth of ultralong CNTs include iron, cobalt,

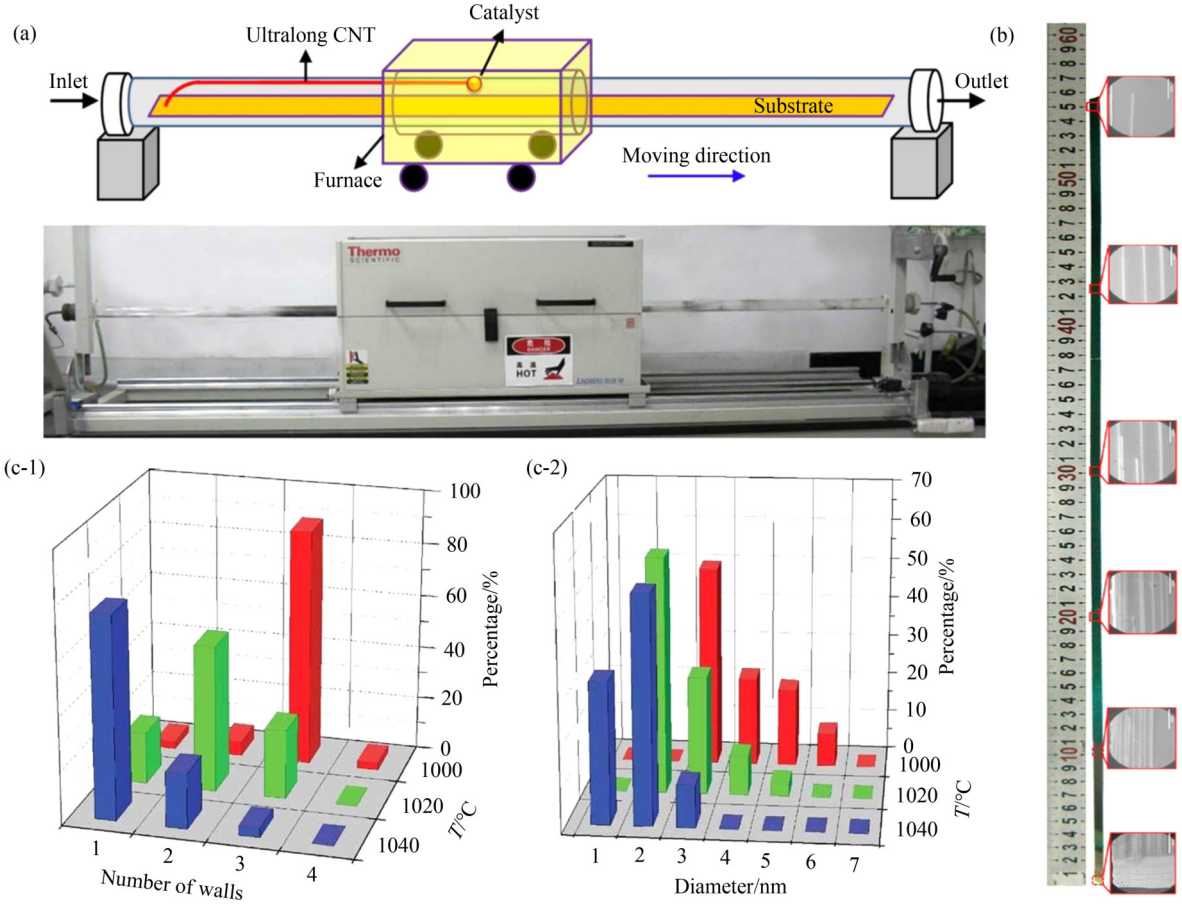

Fig. 5 (a) Furnace-moving method for synthesizing meter-long CNTs. Schematic illustration of a furnace-moving method and optical image of a moving furnace. Synthesis and properties of 550-mm-long CNTs. (b) SEM image of 550 mm long CNTs. Reprinted with permission from Ref. [36], copyright 2013, American Chemical Society. (c) Structure distribution of CNTs grown at different temperatures: (1) Distribution of numbers of walls of centimeter-long CNTs; (2) Distribution of outer diameters of centimeter-long CNTs. Reprinted with permission from Ref. [38], copyright 2010, Wiley-VCH.

copper, cobalt-molybdenum alloys, lead, and various oxides [39−42]. Among these, iron is the most widely employed. The concentration of the precursor solution significantly influences the growth of CNTs, with low concentrations (ranging from 0.001 to 0.1 mol·L^{-1}) [41] typically yielding optimal results. The particle size of the catalyst also plays a critical role in determining growth outcomes. In high-temperature environments, catalysts are prone to aggregation, which can hinder CNT growth. Preventing such aggregation is essential for achieving the growth of high-density and ultralong CNTs [43].

Substrate selection is also a critical factor in the growth of ultralong CNTs. It is commonly observed that silicon wafers with a thin layer of silicon dioxide are particularly well-suited for the growth of gas flow-induced directional CNTs. In contrast, quartz substrates, when combined with carefully controlled growth conditions, can enable the formation of composite horizontal arrays of ultralong CNTs that are influenced by both gas flow and substrate-induced effects [44,45]. By integrating the above factors and optimizing the growth conditions for CNT horizontal arrays through both theoretical and experimental approaches, it is possible to achieve well-aligned, ultralong CNT arrays.

3.2 Control of the wall number and diameter of ultralong CNTs

In practical applications of CNTs, structural control, in addition to length, presents another complex yet critical challenge. Parameters such as the wall number, which refers to the number of concentric graphene layers in a CNT, and the diameter, directly affect the properties of strength, conductivity, and flexibility. Temperature plays a crucial role in defining the wall number and diameter of ultralong CNTs. During their use of the gas flow-induced method for CNT array preparation, Wen et al. [38] found the direct relationship between the number of walls in the CNTs and temperature. As the growth temperature increases, both the number of walls and the CNT diameter decrease. At 1000 °C, the proportion of triple-walled CNTs reached 90%, while at 1020 °C, the proportion of double-walled CNTs surpassed 50%, with triple-walled CNTs comprising approximately 20% (Fig. 5(c)). In the synthesis of ultralong CNTs, Yao et al. [46] investigated the effect of growth temperature variation, observing the formation of intramolecular junctions between CNTs of different diameters. This work provided further evidence of the significant impact of temperature on CNT diameter. Specifically, an increase in reaction temperature leads to a reduction in CNT diameter. This phenomenon is likely attributed to changes in the carbon solubility of the catalyst particles at elevated temperatures, which subsequently alters their shape. Additionally, temperature variations influence the interface interactions between the CNTs and the catalyst.

Catalyst material and size play a pivotal role in determining both the wall number and diameter of CNTs. Metal catalysts, including iron, copper, and cobalt, are commonly employed in the synthesis of CNTs. Among these, copper is particularly advantageous due to its lower melting and boiling points, as well as its weaker interaction with silicon substrates compared to iron, facilitating the growth of CNT horizontal arrays [40]. Both experimental studies and molecular dynamics simulations indicate that variations in surface energy result in smaller and more uniformly distributed copper particles. This leads to the production of CNTs with a narrower and more concentrated diameter distribution when copper is used as the catalyst. Furthermore, by adjusting the concentration of the catalyst precursor, it is possible to control the size of the catalyst particles and, in turn, achieve HACNTs with selectively tailored diameter distributions.

3.3 Control of the areal density of ultralong CNTs

Areal density refers to the number of CNTs per unit area on a substrate, which significantly affects the physical and electrical properties of the resulting CNT films. Beyond the length, diameter, and morphology of CNTs, their density is a crucial parameter for applications in micro- and nanoelectronics. For instance, the fabrication and integration of CNT-based chips require high-purity, high-density semiconductor-type CNT arrays, with a target density of 125 tubes·μm^{-1} [48].

Inhibiting catalyst aggregation at high temperatures is a key approach to enhancing the density of CNT horizontal arrays. Xie et al. [49] demonstrated that introducing silica or graphene into the catalyst region effectively mitigates catalyst particle aggregation, thereby increasing the CNT array density. In their method, silica nanospheres were spin-coated onto the surface of silicon wafers, followed by annealing at a specific temperature to remove residual polymer. A 0.03 mol·L^{-1} $FeCl_3$ solution was then spin-coated to serve as the catalyst. The silicon wafer was placed in a quartz tube, with a second silicon wafer positioned as the substrate for the HACNTs. Their findings confirmed that the presence of silica nanospheres significantly suppressed catalyst aggregation, leading to a marked improvement in the density of the HACNTs.

One effective approach is the careful control of catalyst distribution on the substrate. Hu et al. [50] introduced the “Trojan Catalyst” approach for synthesizing ultralong, high-density single-walled CNT horizontal arrays. This method employed single-crystal alumina as the substrate and involved a pre-treatment step that stored the catalyst within the substrate. During CNT growth, the catalyst was progressively released, which sustained catalytic activity and facilitated the formation of single-walled CNT arrays with ultrahigh densities reaching up to 130 nanotubes per micrometer. Jiang et al. [47] demonstrated

a method to significantly enhance the areal density of ultralong CNT arrays by employing floating bimetallic catalysts synthesized *In situ* within a CVD process (Fig. 6(a)). The Fe-Cu catalyst was found to be particularly effective, increasing the areal density of ultralong CNT arrays to a record-breaking value of about 8100 tubes·mm^{-1}, which was significantly higher than the values typically achieved with single-metal catalysts (Fig. 6(b)). The optimized Fe-Cu catalyst also exhibited a lifetime 3.40 times longer than that of pure Fe catalyst, thus achieving both high yields and uniformity. The introduction of copper into the iron catalyst was shown to improve catalyst fluidity and decrease carbon solubility, which are critical for the continuous and fast growth of ultralong CNTs.

3.4 Control of the morphology of ultralong CNTs

CNTs are often synthesized in agglomerated, randomly aligned structures with extensive entanglement, which significantly impedes both property evaluation and practical applications. Under specific conditions, however, CNTs can be produced in parallel, forming horizontal arrays. The ordered alignment enhances the mechanical, electrical, and optical properties of CNTs, broadening their potential for diverse applications and highlighting their significance in fundamental research.

It is widely accepted that stable gas flow facilitates the directional alignment of ultralong CNTs. The flow direction directly influences the orientation of the CNTs, while disturbances in the flow can cause fluctuations or bending of the nanotubes. To minimize flow disturbances and achieve more stable gas dynamics, Hong et al. [51] introduced a method in which a smaller quartz tube is placed inside a larger one, reducing the Reynolds number and thereby improving the flow conditions. Peng et al. [52] conducted a systematic study on the influence of the Reynolds and Richardson numbers on the growth of ultralong CNTs, concluding that lower Reynolds numbers and higher Richardson numbers promote the floating

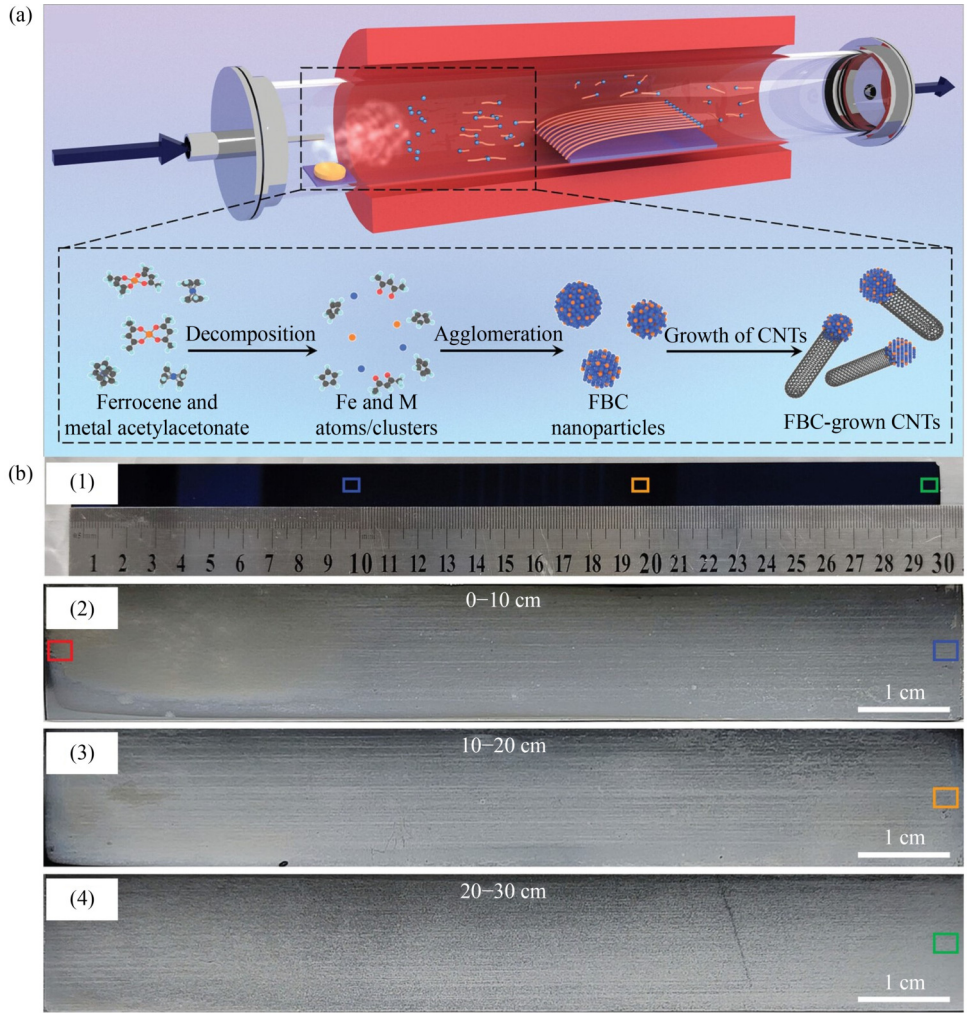

Fig. 6 (a) Schematic illustration of the *in situ* synthesis process of floating bimetallic catalysts and the subsequent growth of ultralong CNTs. (b) Photograph of an ultralong CNT array grown on a 30 cm-long silicon substrate. (2–4) Vapor-condensation-assisted optical images of three segments of the 30 cm-long CNT array (2) 0–10 cm, (3) 10–20 cm, (4) 20–30 cm. Reprinted with permission from Ref. [47], copyright 2024, Wiley-VCH.

growth of these nanotubes.

In summary, controlling the morphology of ultralong CNTs is essential for optimizing their functional properties and applications. Strategies such as substrate selection, adjustment of synthesis parameters, application of external forces, and the use of additives provide researchers with various tools to manipulate CNT morphology. By systematically optimizing these factors, it is possible to achieve high-quality ultralong CNTs with tailored characteristics, enhancing their performance in advanced technological applications.

Considerable progress has been made in the study of ultralong CNTs, particularly in understanding their growth mechanisms, controlled synthesis, and structural and morphological regulation. Despite these advancements, significant challenges remain in the controlled fabrication of ultralong CNTs. Current syntheses still fall short of meeting the requirements for fundamental research and practical applications, particularly in terms of chirality, density, length, and structural uniformity. To overcome these challenges, further research is needed to better understand the growth mechanisms of ultralong CNTs, enhance their density, and achieve controlled synthesis of CNTs with macroscopic lengths and perfect structural properties.

4 Applications of ultralong CNTs

The defect-free structures and macroscopic lengths endow the ultralong CNTs with exceptional properties and novel characteristics. For instance, Wang et al. [53] reported that the ultralong CNTs achieved a uniform and high field effect mobility of 10500 $cm^2 \cdot V^{-1} \cdot s^{-1}$. Bai et al. [3] found that the ultralong CNTs possess a high tensile strength exceeding 100 GPa and can endure more than a hundred million stretching cycles without fracturing. Such properties make ultralong CNTs highly promising for high-end applications, such as carbon-based chips, high-performance sensors, and super-strong fibers. However, due to the immaturity of synthesis techniques for ultralong CNTs in early research, it has been challenging for researchers to obtain high-density ultralong CNT samples, which limited the further exploration of their properties and applications. In recent years, the continuous advancement of the ultralong CNTs' synthesis techniques has motivated researchers to develop several prototype applications based on ultralong CNTs. In the following text, the recent advances of ultralong CNTs' applications in field-effect transistors (FETs), sensors, and photodetectors are introduced.

4.1 Ultralong CNT-based FETs

CNTs are considered to be promising candidates for next-generation high-performance FETs [54]. According to their electronic band structure, CNTs can be classified into metallic and semiconducting types [55]. The metallic CNTs are able to carry current densities up to $10^9 \cdot A \cdot cm^{-2}$, which is higher than that of noble metals [56]. The semiconducting CNTs, with both electron and hole mobility as high as 79000 $cm^2 \cdot V^{-1} \cdot s^{-1}$ due to Dirac fermions, exhibit great potential to replace Si for ultra-scaled logic device application [57]. The controllable synthesis of CNTs with specific structures has been the main obstacle to their application in integrated circuits. Tremendous efforts have been made to achieve semiconducting CNT arrays with a purity as high as 99.9999% and an array density of 125 tubes$\cdot \mu m^{-1}$ [18]. The liquid-phase purification and interface assembly of CNTs are proven to be effective in preparing high-purity and high-density semiconducting CNTs, but the dispersion and separation processes often introduce polymer impurities and defects, which deteriorate the semiconductor devices' performance [58−61]. Besides, the reproducible synthesis of all-semiconducting few-walled CNTs is challenging, as the presence of any metallic inner wall in a few-walled CNT can cause leakage currents and result in a reduced on/off ratio in FET devices [48,62]. Therefore, improving the array density and semiconducting purity during the growth process of CNTs has become a critical challenge for carbon-based electronics fields.

It has been reported that ultralong CNTs synthesized with the assistance of water are predominantly semiconducting [38], indicating their great potential for high-performance FET applications. Zhu et al. [63] reported that the growth rate of semiconducting CNTs was ten times higher than that of metallic CNTs, which led to a spontaneous purification of CNT arrays. Specifically, the purity of semiconducting CNT arrays can reach 99.9999% when the length is over 154 mm. Afterward, they synthesized an ultralong CNT array with length up to 650 mm by catalyst pre-deposition and multiple growths and fabricated FETs on this array with the length over 154 mm (Fig. 7). These devices exhibited a high current of 14 $\mu A \cdot \mu m^{-1}$ with on/off ratio around 10^8 and mobility over 4000 $cm^2 \cdot V^{-1} \cdot s^{-1}$. This work provided a useful strategy to control the CNT purity *in situ* by rate-select growth of ultralong CNT arrays. Similarly, Jiang et al. [37] prepared the ultralong CNT arrays with a high areal density of 6700 tubes$\cdot mm^{-1}$ by SIDS. Large-area FET arrays were fabricated on a 10 cm long CNT sample to evaluate their overall electrical performance (Figs. 8(a–c)). As the array length increased, the proportion of devices with a high on/off ratio also increased, indicating the improved semiconducting CNT purity with longer CNTs (Fig. 8(d)). This result is highly consistent with the aforementioned spontaneous purification phenomena during the growth of ultralong CNTs. Typically, the on/off ratio of pure semiconducting CNT-based FETs is

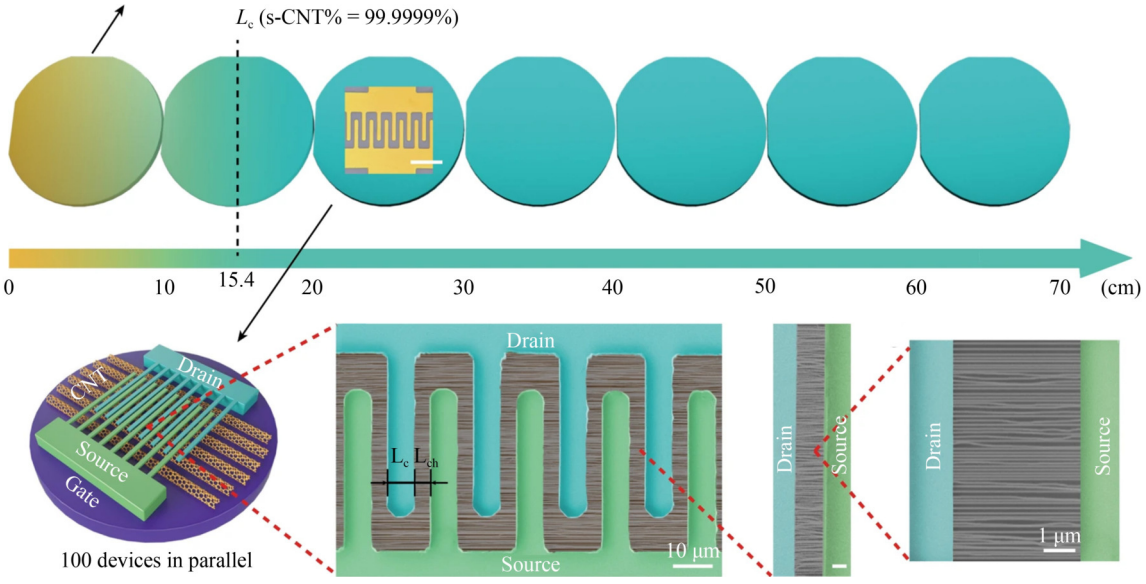

Fig. 7 Schematic illustration of an ultralong CNT array with high semiconducting purity and an interdigitated transistor fabricated on it. Reprinted with permission from Ref. [63], copyright 2019, Springer Nature.

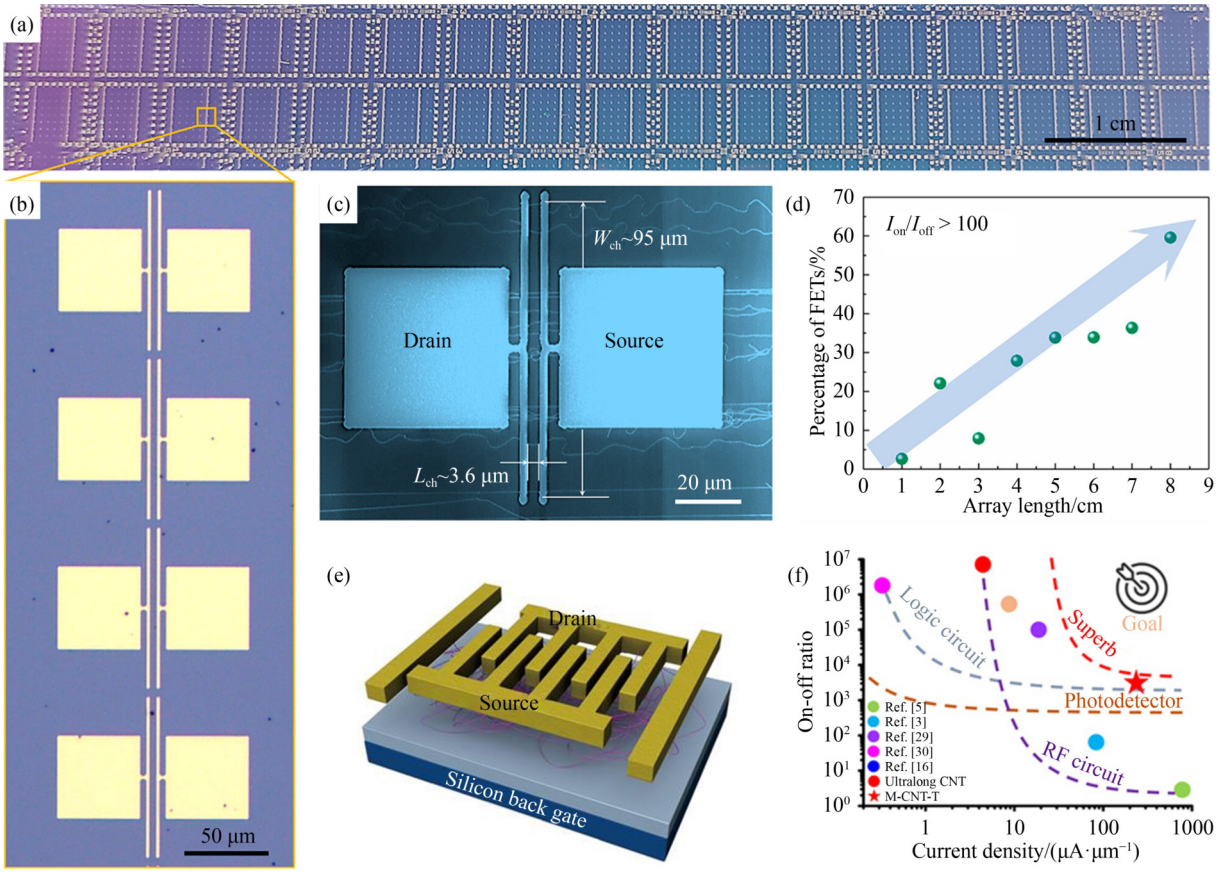

Fig. 8 (a) Optical photograph of the FET devices fabricated on an ultralong CNT array. (b) Optical microscope image and (c) SEM image of the FET devices. (d) The percentage of the FETs with on/off ratios higher than 100 as a function of array length. Reprinted with permission from Ref. [37], copyright 2023, American Chemical Society. (e) Schematic illustration and (f) performances of a back-gated transistor fabricated on the monochromatic CNT tangle. Reprinted with permission from Ref. [64], copyright 2016, American Association for the Advancement of Science.

as high as 4.2×10^5. Moreover, 59.6% and 48.9% of the FET devices demonstrated on/off ratios exceeding 100 and 10000, when the array length reached 8 cm.

Although significant progress has been made in the

in situ synthesis of ultralong CNT arrays with high purity and density, directly synthesizing pure semiconducting CNT arrays with high areal density remains challenging. Even small amounts of metallic CNTs can lead to catastrophic device shorting failures. In this case, Zhu et al. [64] reported an acoustic-assisted assembly of monochromatic CNT tangles to achieve both high purity and density. Specifically, during the growth stage, the monochromatic ultralong CNTs, with lengths of up to 100 μm, self-entangled into tangles *in situ* under the influence of acoustic waves. The prepared CNT tangles consisted of a single CNT, ensuring identical chirality and exhibiting single-color emission under supercontinuum laser illumination. Transistors fabricated on a monochromatic CNT tangle exhibited on/off ratios ranging from 10^3 to 10^6 with 4 mA on-state current, representing the highest recorded value for single CNT-based transistors (Figs. 8(e) and 8(f)). These results highlight the significant potential of ultralong CNTs for high-performance FET applications.

4.2 Ultralong CNT-based sensors

Ultralong CNTs exhibit extraordinary properties, such as immense aspect ratios, high flexibility, ultralight weight, and excellent conductivity. These properties enable their exceptional sensitivity to external fields, positioning them as ideal materials for the construction of high-performance sensors [65]. Cong et al. [66] reported a torsional balance array on a chip with the highest sensitivity level. This remarkable performance was enabled by employing ultralong CNTs as the thread and monolayer graphene coated with aluminum nanofilms as the beam and mirror (Fig. 9(a)). The intrinsic force sensitivity of a torsion balance is proportional to the lengths of the suspension thread but inversely proportional to the fourth power of the diameter of the thread. The ultrahigh aspect ratio and excellent mechanical performances make ultralong CNTs highly promising as suspension threads for high-performance torsion balances. Consequently, torsion balances utilizing ultralong CNTs achieved remarkable sensitivities ranging from 10^{13} to 10^{17} rad·N^{-1} and force measurement in the range of 2×10^{-14} to 2×10^{-18} N.

Moreover, due to their lightweight nature, ultrahigh aspect ratio, and exceptional flexibility, suspended ultralong CNTs can undergo significant deformation and generate substantial electrical signals in response to external stimuli. These characteristics make them ideal building blocks for high-performance airflow sensors [67]. Jiang et al. [31] prepared suspended ultralong CNT networks as high-performance airflow sensors using a one-step FCCVD method. In this approach, ultralong CNTs and short CNTs were *in situ* self-assembled into suspended networks over trenches on silicon substrates (Fig. 9(b)). Subsequently, the networks were decorated with tar nanoparticles to make them visible under optical microscopes and to increase the drag forces of the networks, thereby improving their airflow sensing capabilities. The as-prepared suspended ultralong CNT networks demonstrated exceptional performance, including a record-breaking short response time of 0.021 s, a high detection sensitivity of 0.0124 s·m^{-1}, a small detection threshold of 0.11 m·s^{-1}, and a wide detection range of approximately 0.11–5.51 m·s^{-1}, surpassing to most of the state-of-the-art airflow sensors (Fig. 9(c)). Moreover, they optimized the airflow sensing performance by modulating the network density. It was observed that sensors based on sparse networks exhibited higher sensitivity and lower detection thresholds but a narrower detection range (Fig. 9(d)). These characteristics can be attributed to the greater flexibility of sparse networks, which deform more readily under airflow, resulting in larger electrical responses. However, sparse networks are also more prone to structural failure under strong airflow.

The piezoresistive responses of the suspended ultralong CNT networks were attributed to inter-tube stress at X junctions, which are formed by the overlapping of crossed CNT bundles (Fig. 9(e)). However, the proportion of X junctions in suspended ultralong CNT networks is relatively low (22.8%–30.2%), which constrains further improvements in their sensing performance. Moreover, the inherent structural fragility of suspended ultralong CNT networks severely limits their detection range, presenting significant challenges for their practical application. Therefore, they designed suspended and crossed ultralong CNT networks to increase the areal density of X junctions and structural stability, thereby increasing the overall airflow sensing performance [68]. The suspended and crossed ultralong CNT networks were self-assembled by ultralong CNTs grown in two different directions through a two-step FCCVD method (Figs. 9(f) and 9(g)). The proportion of X junctions in as-prepared crossed ultralong CNT network was significantly increased to 77.3%–89.4%, which was much higher than that of the previous suspended CNT noncrossed networks (22.8%–30.2%). As a result, the crossed ultralong CNT network-based airflow sensor exhibited not only high sensitivity (0.0124 s·m^{-1}), short response time (0.02 s), and low detection threshold (0.02 m·s^{-1}) but also superior robustness and durability.

Ultralong CNTs are also highly promising as conductive layer in transparent flexible electronics due to their macroscale lengths, exceptional flexibility, fatigue resistance, and outstanding electrical properties. However, in conventional growth systems, ultralong CNTs are anchored to the growth substrate by strong van der Waals interactions, necessitating polymer-assisted transfer methods that often introduce contamination [69]. To address this issue, Wang et al. [70] fabricated nearly invisible and transferable suspended ultralong CNT

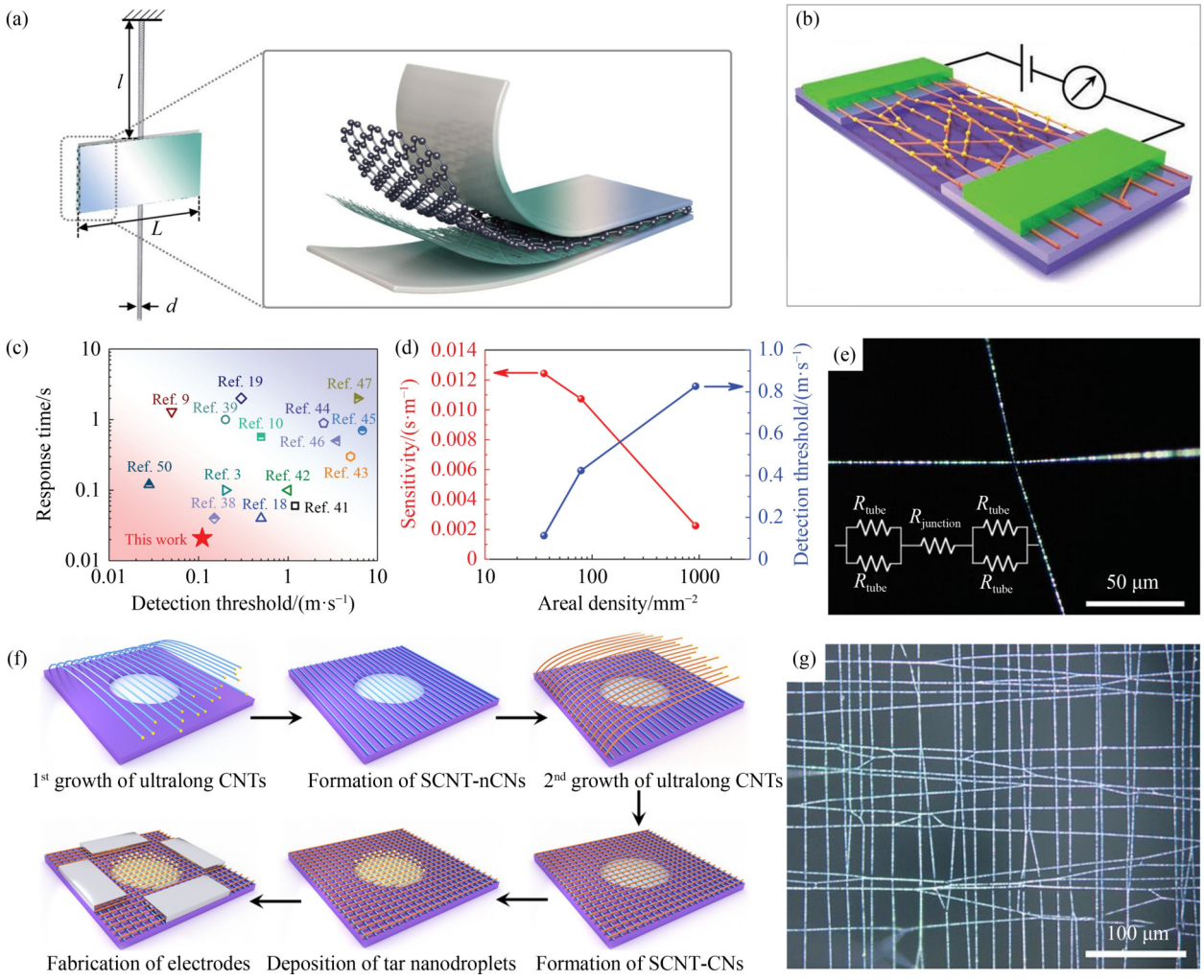

Fig. 9 (a) Schematic illustration of the ultralong CNT-based torsional balance. Reprinted with permission from Ref. [66], copyright 2021, American Association for the Advancement of Science. (b) Schematic illustration of the suspended ultralong CNT-based airflow sensors. (c) Sensing performance comparison of suspended ultralong CNT-based airflow sensors with other airflow sensors. (d) Influence of areal density on the sensitivities and detection thresholds of suspended ultralong CNT-based airflow sensors. (e) Optical microscopy image (inset: equivalent circuit of an X junction) of an X junction in suspended ultralong CNT networks. Reprinted with permission from Ref. [31], copyright 2022, Wiley-VCH. (f) Schematic illustration of the preparation and (g) optical microscopy image of suspended ultralong CNT crossed network-based airflow sensors. Reprinted with permission from Ref. [68], copyright 2024, American Chemical Society.

conductive networks on a centimeter scale (Fig. 10(a)). These suspended ultralong CNT networks can be easily transferred to various target substrates through simple contact, eliminating contamination and demonstrating excellent manipulability (Fig. 10(b)). The centimeter-scale length of ultralong CNTs enabled the efficient assembly of conductive, suspended networks with minimal thickness, reduced absorption area, and low junction density, resulting in exceptional transmittance (> 99% at 550 nm) and transferability. Subsequently, they integrated the ultralong CNT networks onto patterned poly(dimethylsiloxane) films to construct transparent pressure sensors, which only resulted in a negligible degradation (0.36%) of the device's transmittance (Fig. 10(c)). The as-prepared pressure sensor demonstrated a high sensitivity (225.11 kPa^{-1}), a broad operating range (up to 160 kPa), a rapid response time (11 ms), and a robust stability over 10000 cycles (Fig. 10(d)).

Typically, ultralong CNTs consist of two coaxial shells with different diameters. The inter-shell sliding behavior of these CNTs can also be exploited to construct tensile sensors. Wang et al. [71] revealed the reversible and linear electromechanical response to inter-shell sliding in ultralong CNTs (Fig. 10(e)). During the axial stretching, the outer shell of the CNT was broken and the inner shell was pulled out, leading to an increased resistance. The increase was primarily due to inter-shell tunneling, and the electrical current linearly dependent on the inner shell's pull-out distance. This reversible and linear electrical response of ultralong few-walled CNTs made them highly suitable for constructing flexible strain

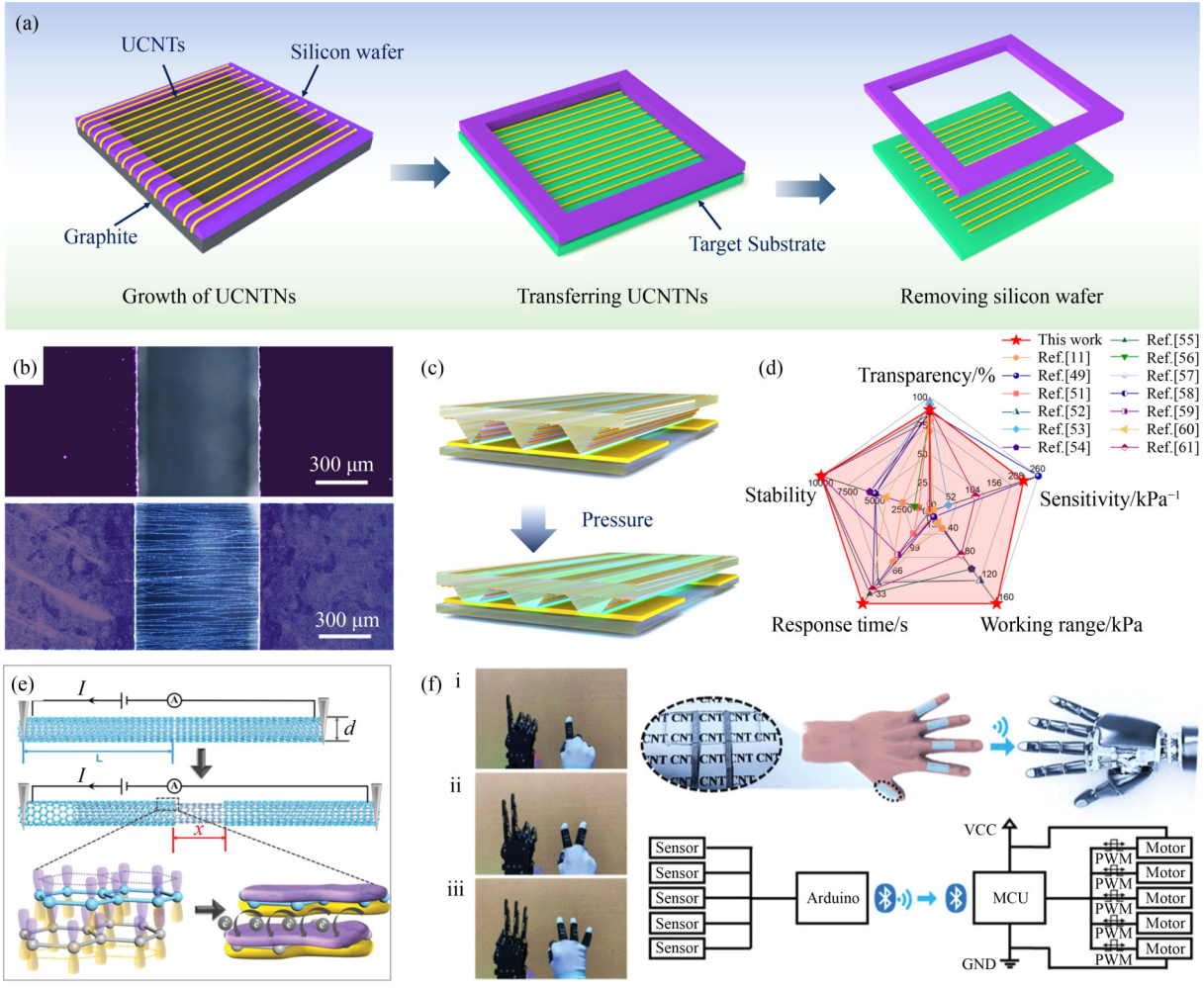

Fig. 10 (a) Schematic illustration of the synthesis and transfer process of suspended ultralong CNT network. (b) Optical micrographs of the silicon wafer with a gap before and after transferring the suspended ultralong CNT network, which was subsequently deposited with tar nanoparticles. (c) Schematic illustration of the ultralong CNT-based pressure sensor's working mechanism. (d) Comparison of the comprehensive sensing performances of the ultralong CNT-based pressure sensor with other transparent flexible pressure sensors. Reprinted with permission from Ref. [70], copyright 2024, American Chemical Society. (e) Schematic illustration of the mechanism for the electrical conductivity variation versus inter-shell sliding of an ultralong CNT. (f) The human-machine interface application ultralong CNT-based tensile sensors of Reprinted with permission from Ref. [71], copyright 2023, Wiley-VCH.

sensors. Therefore, they encapsulated ultralong CNTs into plastic flexible films to fabricate flexible devices and demonstrated its application in human-machine interface (Fig. 10(f)).

4.3 Ultralong CNT-based photodetectors

CNTs are highly promising for high-performance photodetectors under ambient conditions, owing to their ultrabroad absorption spectrum, ultrafast exciton generation processes, tunable band gap, and high carrier mobility [72−77]. However, the performance of previously reported CNT-based photodetectors is often limited by several factors. Structural defects in CNTs can lead to significant electron scattering, drastically reducing mobility. Additionally, interfacial capacitances at CNT junctions severely hinder response speed [78]. In contrast, ultralong CNTs, with their nearly perfect atomic structure and macroscale length, present a highly promising solution for high-performance photodetectors. Wei et al. [79] reported an ultralong CNT photodetector with a diode configuration, achieved by applying n-type (Sc) and p-type (Pd) electrodes at opposite ends of the CNT channel (Fig. 11(a)). This photodetector demonstrated a linear photocurrent under the laser power density ranging from 10^{-1} to 10^{5} W·cm^{-2}. Additionally, the ultralong CNT photodetector maintained a continuous response for incident wavelength from 1165 to 2100 nm. These results highlighted the promising potential of ultralong CNTs for robust, wide-bandwidth light sensing applications.

Moreover, the bolometric effects of CNTs often produce currents that counteract photoconductive effects, thereby reducing the overall photoconductive response [80]. Additionally, the substrates of photodetectors

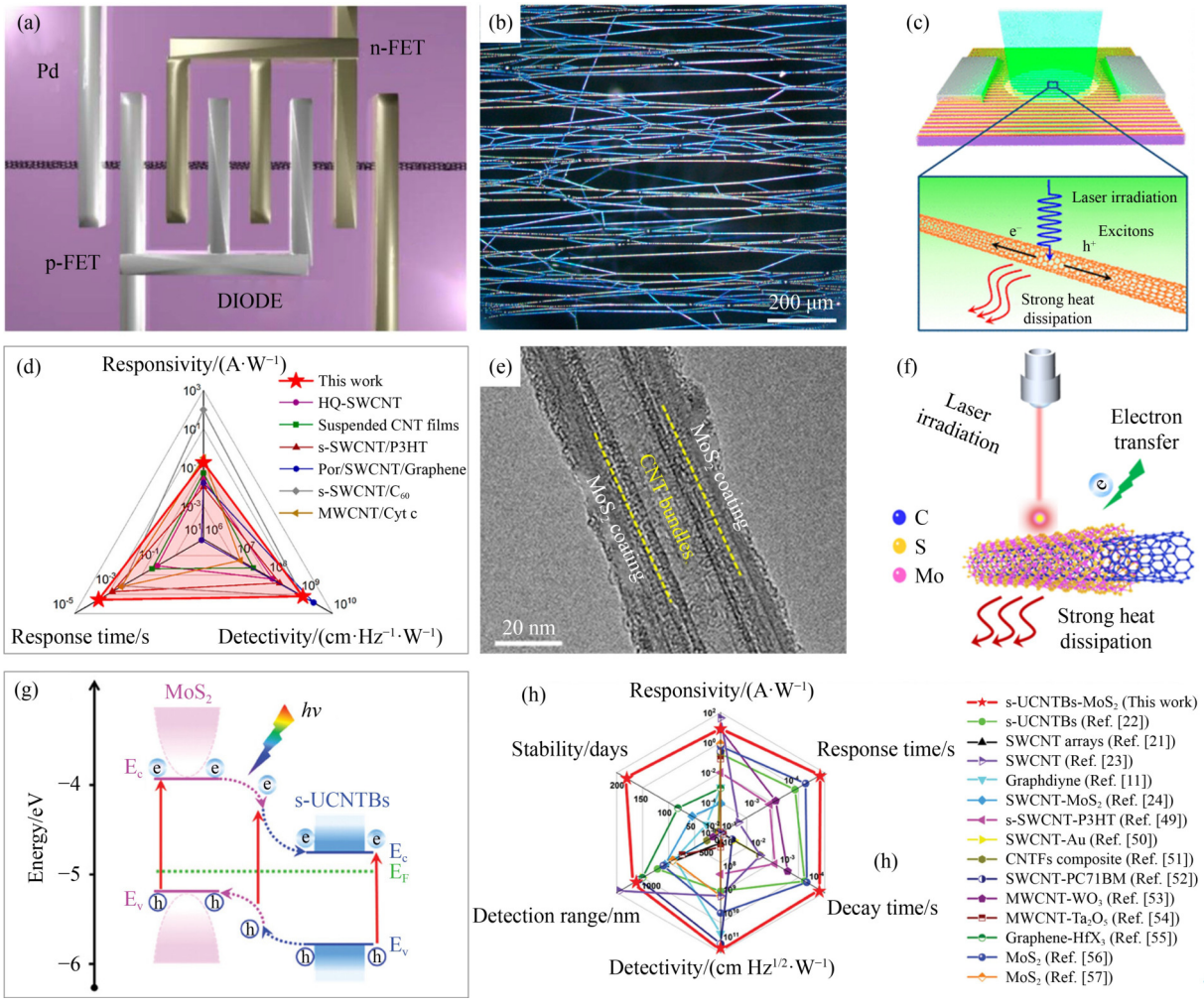

Fig. 11 (a) Schematic illustration of an ultralong CNT-based photodetector with a diode configuration. Reprinted with permission from Ref. [79], copyright 2014, AIP Publishing LLC. (b) Optical micrographs and (c) schematic illustration of suspended ultralong CNT-based photodetector. (d) Performance comparison between suspended ultralong CNT network-based photodetectors and other carbon-based photodetectors. Reprinted with permission from Ref. [83], copyright 2024, American Chemical Society. (e) Transmission electron microscopic images of the ultralong CNT-MoS_2 heterojunction. (f) Photoelectric sensing mechanism and (g) energy band diagram of the suspended ultralong CNT-MoS_2-based photodetector. (h) Performance comparison between ultralong CNT-MoS_2-based photodetector and other reported carbon-based, MoS_2-based photodetectors. Reprinted with permission from Ref. [90], copyright 2024, Wiley-VCH.

typically induce interactions between photoinduced electron-hole pairs and surface polar phonons, which significantly impair carrier mobility [81,82]. Jiang et al. [83] developed high-performance photodetectors utilizing suspended ultralong CNTs (Fig. 11(b)). The unique suspended design not only effectively eliminated substrate interference but also enhanced heat dissipation from CNTs to the surroundings which effectively suppressed the bolometric effects (Fig. 11(c)). As a result, the suspended ultralong CNT-based photodetectors demonstrated outstanding performance, including high responsivity (0.181 $A \cdot W^{-1}$) and detectivity (1.20×10^9 $cm \cdot Hz^{1/2} \cdot W^{-1}$), ultrafast response (0.13 ms), and broad detection range (405–850 nm), outperforming most previously reported nonsuspended CNTs and other nanocarbon material-based photodetectors (Fig. 11(d)). This work revealed the great potential of ultralong CNTs in constructing high-performance photodetectors. However, the photoexcitation of CNTs occurs in the form of electron-hole pair excitons with a strong binding energy (~0.4 eV) [84]. Therefore, achieving a large photoconductive response in pristine CNTs often requires the application of a high bias voltage to dissociate the excitons. Consequently, CNT-based photodetectors often exhibit suboptimal performance due to the limited photothermal conversion efficiency [85,86]. Decorating CNTs with other nanomaterials to construct heterojunction interfaces is a practical strategy to enhance the separation efficiency of electron-hole pairs [87,88]. Such one-dimensional van der Waals heterostructures can exhibit unique physical properties due to the constraints of curvature and diameter, as well as the synergistic effects

of the shell materials [89]. Wang et al. [90] fabricated core-shell-structured suspended ultralong CNT-MoS_2 heterojunction networks via CVD (Fig. 11(e)). The built-in electric field at this heterojunction interface can effectively facilitate the transport and separation of photogenerated electron-hole pairs, thereby enhancing the performance of the photodetector (Figs. 11(f) and 11(g)). The photodetectors based on suspended ultralong CNT-MoS_2 heterojunction networks exhibited outstanding optoelectronic performance, including ultrafast response (0.03 ms), high responsivity (8.51 $A \cdot W^{-1}$), high detectivity (3.74×10^{11} $cm \cdot Hz^{1/2} \cdot W^{-1}$), broad response range (405–1064 nm), and excellent stability (> 200 days). These comprehensive properties significantly surpass those of the previously reported suspended ultralong CNT network-based photodetectors (Fig. 11(h)).

5 Conclusions and outlook

In this review, we have summarized recent advancements in growth mechanisms, controlled synthesis, and diverse applications of ultralong CNTs. Significant progress has been made toward synthesizing ultralong CNTs with well-controlled structures and high yields, with the ultimate goal of enabling their practical use in cutting-edge fields. As for the growth mechanism, we discussed in detail the kite-like growth mode of ultralong CNTs and the thermal effects of substrates, offering deeper insights into their growth behavior. Moreover, the recently developed SIDS has significantly enhanced the yield of ultralong CNTs, unlocking their potential in more applications, including high-performance airflow sensors, photodetectors, and large-area FETs. Despite these advances, the current highest density of ultralong CNT arrays is only 8 tubes·μm^{-1}, which is far below the target of 125 tubes·μm^{-1} required for carbon-based integrated circuits. Furthermore, achieving macroscale applications of ultralong CNTs, such as super-strong fibers and transparent conductive films, remains a formidable challenge. These limitations underscore the substantial obstacles that must be overcome to fully realize the potential of ultralong CNTs. Here, we conclude with the following outlooks for future research and development in this field.

First, the reproducibility of ultralong CNTs' preparations needed to be improved. The synthesis of ultralong CNTs requires extremely stringent growth conditions, where even minor disturbances can lead to a decline in the quality of the ultralong CNTs. This unfavorable phenomenon significantly impedes advancements in research on ultralong CNTs. Employing artificial intelligence-driven robots to fully automate the experimental process can effectively minimize deviations caused by human intervention, thereby significantly improving the controllability and reproducibility of ultralong CNT synthesis. Besides, more insight should be provided into the growth mechanism of ultralong CNTs to help us analyze the critical factors for their controllable synthesis. The integration of high-throughput characterization with artificial intelligence-based annotation techniques can efficiently process and analyze substantial experimental data, enabling in-depth and multidimensional analysis. This approach holds great promise for uncovering novel growth mechanisms of ultralong CNTs.

Second, the FCCVD system has proven effective in synthesizing ultralong CNTs, demonstrating significant potential for large-scale production. However, the current yield remains extremely low, as only a small fraction of CNTs is captured by the substrate and grows into ultralong structures. The low yield of ultralong CNTs remains the primary obstacle hindering their practical application. The optimization of the flow field and temperature field is considered critical to improving interception efficiency, optimizing the growth environment, and achieving higher yields of ultralong CNTs. Flow field and temperature field simulation technologies can provide theoretical guidance for the rational design of reactors and interception substrates.

Finally, although several ultralong CNT-based devices have been reported, the applications based on ultralong CNTs are still in the early stages of development, leaving significant opportunities for further exploration. For instance, the extensive specific surface area and suspended structure of ultralong CNT networks offer significant advantages for gas adsorption, positioning them as highly promising candidates for high-performance gas sensors. Besides, future efforts should focus on functionalization strategies such as *in situ* modification and heterojunction fabrication, according to the requirements of different fields. These approaches impart additional functionalities to ultralong CNTs, paving the way for their widespread application in cutting-edge fields and broadening their potential applications.

Acknowledgements This work is supported by the National Key Research and Development Program (Grant Nos. 2020YFC2201103 and 2020YFA0210702) and the National Natural Science Foundation of China (Grant No. 22075163).

Competing interests The authors declare that they have no competing interests.

References

1. Iijima S. Helical microtubules of graphitic carbon. Nature, 1991, 354(6348): 56–58
2. Zhang R, Zhang Y, Wei F. Horizontally aligned carbon nanotube arrays: growth mechanism, controlled synthesis, characterization, properties and applications. Chemical Society Reviews, 2017,

46(12): 3661–3715
3. Bai Y, Yue H, Wang J, Shen B, Sun S, Wang S, Wang H, Li X, Xu Z, Zhang R, et al. Super-durable ultralong carbon nanotubes. Science, 2020, 369(6507): 1104–1106
4. Bai Y, Zhang R, Ye X, Zhu Z, Xie H, Shen B, Cai D, Liu B, Zhang C, Jia Z, et al. Carbon nanotube bundles with tensile strength over 80 GPa. Nature Nanotechnology, 2018, 13(7): 589–595
5. Zhang X, Lu W, Zhou G, Li Q. Understanding the mechanical and conductive properties of carbon nanotube fibers for smart electronics. Advanced Materials, 2020, 32(5): 1902028
6. Gong Y, Adhikari P, Liu Q, Wang T, Gong M, Chan W L, Ching W Y, Wu J. Designing the interface of carbon nanotube/biomaterials for high-performance ultra-broadband photodetection. ACS Applied Materials & Interfaces, 2017, 9(12): 11016–11024
7. Ackermann J, Metternich J T, Herbertz S, Kruss S. Biosensing with fluorescent carbon nanotubes. Angewandte Chemie International Edition, 2022, 61(18): e202112372
8. Chen Y, Zhang H B, Yang Y, Wang M, Cao A, Yu Z Z. High-performance epoxy nanocomposites reinforced with three-dimensional carbon nanotube sponge for electromagnetic interference shielding. Advanced Functional Materials, 2016, 26(3): 447–455
9. Chen S, Qiu L, Cheng H M. Carbon-based fibers for advanced electrochemical energy storage devices. Chemical Reviews, 2020, 120(5): 2811–2878
10. Li R, Jiang Q, Zhang R. Progress and perspective on high-strength and multifunctional carbon nanotube fibers. Science Bulletin, 2022, 67(8): 784–787
11. Sun D M, Timmermans M Y, Kaskela A, Nasibulin A G, Kishimoto S, Mizutani T, Kauppinen E I, Ohno Y. Mouldable all-carbon integrated circuits. Nature Communications, 2013, 4(1): 2302
12. Chen T, Dai L. Flexible supercapacitors based on carbon nanomaterials. Journal of Materials Chemistry A: Materials for Energy and Sustainability, 2014, 2(28): 10756–10775
13. Huang J, Zhang Q, Zhao M, Wei F. A review of the large-scale production of carbon nanotubes: the practice of nanoscale process engineering. Chinese Science Bulletin, 2012, 57(2): 157–166
14. Zhang X, Lei X, Jia X, Sun T, Luo J, Xu S, Li L, Yan D, Shao Y, Yong Z, et al. Carbon nanotube fibers with dynamic strength up to 14 GPa. Science, 2024, 384(6702): 1318–1323
15. Yang Z, Tian J, Yin Z, Cui C, Qian W, Wei F. Carbon nanotube- and graphene-based nanomaterials and applications in high-voltage supercapacitor: a review. Carbon, 2019, 141: 467–480
16. Wei F, Zhang Q, Qian W Z, Yu H, Wang Y, Luo G H, Xu G H, Wang D Z. The mass production of carbon nanotubes using a nano-agglomerate fluidized bed reactor: a multiscale space-time analysis. Powder Technology, 2008, 183(1): 10–20
17. Cho W, Schulz M, Shanov V. Growth and characterization of vertically aligned centimeter long cnt arrays. Carbon, 2014, 72: 264–273
18. Tulevski G S, Franklin A D, Frank D, Lobez J M, Cao Q, Park H, Afzali A, Han S J, Hannon J B, Haensch W. Toward high-performance digital logic technology with carbon nanotubes. ACS Nano, 2014, 8(9): 8730–8745
19. Kong J, Soh H T, Cassell A M, Quate C F, Dai H. Synthesis of individual single-walled carbon nanotubes on patterned silicon wafers. Nature, 1998, 395(6705): 878–881
20. Iijima S, Ichihashi T. Single-shell carbon nanotubes of 1-Nm diameter. Nature, 1993, 363(6430): 603–605
21. Guo T, Nikolaev P, Rinzler A G, Tomanek D, Colbert D T, Smalley R E. Self-assembly of tubular fullerenes. Journal of Physical Chemistry, 1995, 99(27): 10694–10697
22. Thess A, Lee R, Nikolaev P, Dai H, Petit P, Robert J, Xu C, Lee Y H, Kim S G, Rinzler A G, et al. Crystalline ropes of metallic carbon nanotubes. Science, 1996, 273(5274): 483–487
23. Gavillet J, Loiseau A, Journet C, Willaime F, Ducastelle F, Charlier J C. Root-growth mechanism for single-wall carbon nanotubes. Physical Review Letters, 2001, 87(27): 275504
24. Zhang R, Xie H, Zhang Y, Zhang Q, Jin Y, Li P, Qian W, Wei F. The reason for the low density of horizontally aligned ultralong carbon nanotube arrays. Carbon, 2013, 52: 232–238
25. Yoshida H, Takeda S, Uchiyama T, Kohno H, Homma Y. Atomic-scale in-situ observation of carbon nanotube growth from solid state iron carbide nanoparticles. Nano Letters, 2008, 8(7): 2082–2086
26. He M, Duan X, Wang X, Zhang J, Liu Z, Robinson C. Iron catalysts reactivation for efficient CVD growth of SWNT with base-growth mode on surface. Journal of Physical Chemistry B, 2004, 108(34): 12665–12668
27. Helveg S, López-Cartes C, Sehested J, Hansen P L, Clausen B S, Rostrup-Nielsen J R, Abild-Pedersen F, Nørskov J K. Atomic-scale imaging of carbon nanofibre growth. Nature, 2004, 427(6973): 426–429
28. Ago H, Ishigami N, Yoshihara N, Imamoto K, Akita S, Ikeda K I, Tsuji M, Ikuta T, Takahashi K. Visualization of horizontally-aligned single-walled carbon nanotube growth with $^{13}C/^{12}C$ isotopes. Journal of Physical Chemistry C, 2008, 112(6): 1735–1738
29. Zhang R, Zhang Y, Xie H, Zhang Q, Qian W, Wei F. Controlled synthesis and property of horizontally aligned carbon nanotubes. Scientia Sinica Chimica, 2015, 45(10): 979–1009
30. Jiang Q, Wang F, Li R, Wu X, Zhang W, Zhao S, Huang Y, Wang B, Zhang S, Zhao Y, et al. The inherent thermal effect of substrates on the growth of ultralong carbon nanotubes. Advanced Functional Materials, 2022, 33(10): 2212665
31. Jiang Q, Li R, Wang F, Shi X, Chen F, Huang Y, Wang B, Zhang W, Wu X, Wei F, et al. Ultrasensitive airflow sensors based on suspended carbon nanotube networks. Advanced Materials, 2022, 34(18): 2107062
32. Hofmann M, Nezich D, Reina A, Kong J. In-situ sample rotation as a tool to understand chemical vapor deposition growth of long aligned carbon nanotubes. Nano Letters, 2008, 8(12): 4122–4127
33. Ma Y, Wang B, Wu Y, Huang Y, Chen Y. The production of horizontally aligned single-walled carbon nanotubes. Carbon, 2011, 49(13): 4098–4110
34. Jian M, Xie H, Wang Q, Xia K, Yin Z, Zhang M, Deng N, Wang L, Ren T, Zhang Y. Volatile-nanoparticle-assisted optical visualization of individual carbon nanotubes and other nanomaterials. Nanoscale, 2016, 8(27): 13437–13444

35. Flory P J. Molecular size distribution in linear condensation polymers. Journal of the American Chemical Society, 1936, 58(10): 1877–1885
36. Zhang R, Zhang Y, Zhang Q, Xie H, Qian W, Wei F. Growth of half-meter long carbon nanotubes based on Schulz-Flory distribution. ACS Nano, 2013, 7(7): 6156–6161
37. Jiang Q, Wang F, Li R, Li B, Wei N, Gao N, Xu H, Zhao S, Huang Y, Wang B, et al. Synthesis of ultralong carbon nanotubes with ultrahigh yields. Nano Letters, 2023, 23(2): 523–532
38. Wen Q, Qian W, Nie J, Cao A, Ning G, Wang Y, Hu L, Zhang Q, Huang J, Wei F. 100 mm long, semiconducting triple-walled carbon nanotubes. Advanced Materials, 2010, 22(16): 1867–1871
39. Huang S, Cai X, Liu J. Growth of millimeter-long and horizontally aligned single-walled carbon nanotubes on flat substrates. Journal of the American Chemical Society, 2003, 125(19): 5636–5637
40. Cui R, Zhang Y, Wang J, Zhou W, Li Y. Comparison between copper and iron as catalyst for chemical vapor deposition of horizontally aligned ultralong single-walled carbon nanotubes on silicon substrates. Journal of Physical Chemistry C, 2010, 114(37): 15547–15552
41. Reina A, Hofmann M, Zhu D, Kong J. Growth mechanism of long and horizontally aligned carbon nanotubes by chemical vapor deposition. Journal of Physical Chemistry C, 2007, 111(20): 7292–7297
42. Zhou W, Han Z, Wang J, Zhang Y, Jin Z, Sun X, Zhang Y, Yan C, Li Y. Copper catalyzing growth of single-walled carbon nanotubes on substrates. Nano Letters, 2006, 6(12): 2987–2990
43. Wang Q, Ng M F, Yang S W, Yang Y, Chen Y. The mechanism of single-walled carbon nanotube growth and chirality selection induced by carbon atom and dimer addition. ACS Nano, 2010, 4(2): 939–946
44. Zhang B, Hong G, Peng B, Zhang J, Choi W, Kim J M, Choi J Y, Liu Z. Grow single-walled carbon nanotubes cross-bar in one batch. Journal of Physical Chemistry C, 2009, 113(14): 5341–5344
45. Liu Z, Jiao L, Yao Y, Xian X, Zhang J. Aligned, ultralong single-walled carbon nanotubes: from synthesis, sorting, to electronic devices. Advanced Materials, 2010, 22(21): 2285–2310
46. Yao Y, Li Q, Zhang J, Liu R, Jiao L, Zhu Y T, Liu Z. Temperature-mediated growth of single-walled carbon-nanotube intramolecular junctions. Nature Materials, 2007, 6(4): 283–286
47. Jiang Q, Wu Y, Wang F, Zhu P, Li R, Zhao Y, Huang Y, Wu X, Zhao S, Li Y, et al. Floating bimetallic catalysts for growing 30 cm-long carbon nanotube arrays with high yields and uniformity. Advanced Materials, 2024, 36(32): 2402257
48. Franklin A D. The road to carbon nanotube transistors. Nature, 2013, 498(7455): 443–444
49. Xie H, Zhang R, Zhang Y, Li P, Jin Y, Wei F. Growth of high-density parallel arrays of ultralong carbon nanotubes with catalysts pinned by silica nanospheres. Carbon, 2013, 52: 535–540
50. Hu Y, Kang L, Zhao Q, Zhong H, Zhang S, Yang L, Wang Z, Lin J, Li Q, Zhang Z, et al. Growth of high-density horizontally aligned SWNT arrays using Trojan catalysts. Nature Communications, 2015, 6(1): 6099
51. Hong B H, Lee J Y, Beetz T, Zhu Y, Kim P, Kim K S. Quasi-continuous growth of ultralong carbon nanotube arrays. Journal of the American Chemical Society, 2005, 127(44): 15336–15337
52. Peng B, Yao Y, Zhang J. Effect of the Reynolds and Richardson numbers on the growth of well-aligned ultralong single-walled carbon nanotubes. Journal of Physical Chemistry C, 2010, 114(30): 12960–12965
53. Wang X, Li Q, Xie J, Jin Z, Wang J, Li Y, Jiang K, Fan S. Fabrication of ultralong and electrically uniform single-walled carbon nanotubes on clean substrates. Nano Letters, 2009, 9(9): 3137–3141
54. Brady G J, Way A J, Safron N S, Evensen H T, Gopalan P, Arnold M S. Quasi-ballistic carbon nanotube array transistors with current density exceeding Si and GaAs. Science Advances, 2016, 2(9): e1601240
55. Qiu L, Ding F. Understanding single-walled carbon nanotube growth for chirality controllable synthesis. Accounts of Materials Research, 2021, 2(9): 828–841
56. Wei B Q, Vajtai R, Ajayan P M. Reliability and current carrying capacity of carbon nanotubes. Applied Physics Letters, 2001, 79(8): 1172–1174
57. Wehling T O, Black-Schaffer A M, Balatsky A V. Dirac materials. Advances in Physics, 2014, 63(1): 1–76
58. Liu L, Han J, Xu L, Zhou J, Zhao C, Ding S, Shi H, Xiao M, Ding L, Ma Z, et al. Aligned, high-density semiconducting carbon nanotube arrays for high-performance electronics. Science, 2020, 368(6493): 850–856
59. Ghosh S, Bachilo S M, Weisman R B. Advanced sorting of single-walled carbon nanotubes by nonlinear density-gradient ultracentrifugation. Nature Nanotechnology, 2010, 5(6): 443–450
60. Cao Q, Han S J, Tulevski G S, Zhu Y, Lu D D, Haensch W. Arrays of single-walled carbon nanotubes with full surface coverage for high-performance electronics. Nature Nanotechnology, 2013, 8(3): 180–186
61. Nish A, Hwang J Y, Doig J, Nicholas R J. Highly selective dispersion of single-walled carbon nanotubes using aromatic polymers. Nature Nanotechnology, 2007, 2(10): 640–646
62. Avouris P, Chen Z, Perebeinos V. Carbon-based electronics. Nature Nanotechnology, 2007, 2(10): 605–615
63. Zhu Z, Wei N, Cheng W, Shen B, Sun S, Gao J, Wen Q, Zhang R, Xu J, Wang Y, et al. Rate-selected growth of ultrapure semiconducting carbon nanotube arrays. Nature Communications, 2019, 10(1): 4467
64. Zhu Z, Wei N, Xie H, Zhang R, Bai Y, Wang Q, Zhang C, Wang S, Peng L, Dai L, et al. Acoustic-assisted assembly of an individual monochromatic ultralong carbon nanotube for high on-current transistors. Science Advances, 2016, 2(11): e1601572
65. Wang K, Wang F, Jiang Q, Zhu P, Leu K, Zhang R. Controlled synthesis, properties, and applications of ultralong carbon nanotubes. Nanoscale Advances, 2024, 6(18): 4504–4521
66. Cong L, Yuan Z, Bai Z, Wang X, Zhao W, Gao X, Hu X, Liu P, Guo W, Li Q, et al. On-chip torsion balances with femtonewton force resolution at room temperature enabled by carbon nanotube and graphene. Science Advances, 2021, 7(12): eabd2358
67. Dresselhaus M S, Dresselhaus G, Jorio A. Unusual properties and structure of carbon nanotubes. Annual Review of Materials

Research, 2004, 34(1): 247–278
68. Jiang Q, Leu K, Gong X, Wang F, Li R, Wang K, Zhu P, Zhao Y, Zang Y, Zhang R. High-performance airflow sensors based on suspended ultralong carbon nanotube crossed networks. ACS Applied Materials & Interfaces, 2024, 16(16): 20949–20958
69. Jiao L, Xian X, Liu Z. Manipulation of ultralong single-walled carbon nanotubes at macroscale. Journal of Physical Chemistry C, 2008, 112(27): 9963–9965
70. Wang F, Wang K, Chang Z, Liang H, Jiang Q, Xi A, Zhao Y, Zhao S, Leu K, Wu X, et al. Highly transparent and transferable ultralong carbon nanotube networks for transparent wearable electronics. ACS Nano, 2024, 18(48): 33245–33255
71. Wang H, Jian M, Li S, Liang X, Lu H, Xia K, Zhu M, Wu Y, Zhang Y. Inter-shell sliding in individual few-walled carbon nanotubes for flexible electronics. Advanced Materials, 2023, 35(48): 2306144
72. He X, Léonard F, Kono J. Uncooled carbon nanotube photodetectors. Advanced Optical Materials, 2015, 3(8): 989–1011
73. Dürkop T, Getty S A, Cobas E, Fuhrer M S. Extraordinary mobility in semiconducting carbon nanotubes. Nano Letters, 2004, 4(1): 35–39
74. Burdanova M G, Tsapenko A P, Kharlamova M V, Kauppinen E I, Gorshunov B P, Kono J, Lloyd-Hughes J. A review of the terahertz conductivity and photoconductivity of carbon nanotubes and heteronanotubes. Advanced Optical Materials, 2021, 9(24): 2101042
75. Pop E, Mann D A, Goodson K E, Dai H. Electrical and thermal transport in metallic single-wall carbon nanotubes on insulating substrates. Journal of Applied Physics, 2007, 101(9): 093710
76. Freitag M, Martin Y, Misewich J A, Martel R, Avouris P. Photoconductivity of single carbon nanotubes. Nano Letters, 2003, 3(8): 1067–1071
77. Itkis M E, Borondics F, Yu A, Haddon R C. Bolometric infrared photoresponse of suspended single-walled carbon nanotube films. Science, 2006, 312(5772): 413–416
78. Yu L, Shearer C, Shapter J. Recent development of carbon nanotube transparent conductive films. Chemical Reviews, 2016, 116(22): 13413–13453
79. Wei N, Liu Y, Xie H, Wei F, Wang S, Peng L M. Carbon nanotube light sensors with linear dynamic range of over 120 dB. Applied Physics Letters, 2014, 105(7): 073107
80. Zhu J L, Zhang G, Wei J, Sun J L. Negative and positive photoconductivity modulated by light wavelengths in carbon nanotube film. Applied Physics Letters, 2012, 101(12): 123117
81. Low T, Perebeinos V, Kim R, Freitag M, Avouris P. Cooling of photoexcited carriers in graphene by internal and substrate phonons. Physical Review B: Condensed Matter and Materials Physics, 2012, 86(4): 045413
82. Wang H D, Liu J H, Guo Z Y, Zhang X, Zhang R F, Wei F, Li T Y. Thermal transport across the interface between a suspended single-walled carbon nanotube and air. Nanoscale and Microscale Thermophysical Engineering, 2013, 17(4): 349–365
83. Jiang Q, Wang K, Wang F, Leu K, Li R, Zhao Y, Xi A, Zang Y, Zhang R. High-performance photodetectors based on suspended ultralong carbon nanotubes. ACS Nano, 2024, 18(36): 25249–25256
84. Zheng Z, Fang H, Liu D, Tan Z, Gao X, Hu W, Peng H, Tong L, Hu W, Zhang J. Nonlocal response in infrared detector with semiconducting carbon nanotubes and graphdiyne. Advanced Science, 2017, 4(12): 1700472
85. Zeng Q, Wang S, Yang L, Wang Z, Pei T, Zhang Z, Peng L M, Zhou W, Liu J, Zhou W, et al. Carbon nanotube arrays based high-performance infrared photodetector. Optical Materials Express, 2012, 2(6): 839–848
86. Chen C, Zhao Y M, Yu H L, Jiao X Y, Hu X G, Li X, Hou P X, Liu C, Cheng H M. High-performance infrared photodetector based on single-wall carbon nanotube films. Carbon, 2023, 206: 150–156
87. Wang H, Li Z, Li D, Chen P, Pi L, Zhou X, Zhai T. Van der Waals integration based on two-dimensional materials for high-performance infrared photodetectors. Advanced Functional Materials, 2021, 31(30): 2103106
88. Huang P Y, Chen H J, Qin J K, Zhen L, Xu C Y. A polarization-sensitive photothermoelectric photodetector based on mixed-dimensional SWCNT-MoS_2 heterostructures. Nanoscale Advances, 2022, 4(24): 5290–5296
89. Xiang R, Inoue T, Zheng Y, Kumamoto A, Qian Y, Sato Y, Liu M, Tang D, Gokhale D, Guo J, et al. One-dimensional van der Waals heterostructures. Science, 2020, 367(6477): 537–542
90. Wang K, Wang F, Cao Y, Jiang Q, Xi A, Leu K, Wang X, Zang Y, Liu R, Zhang R. High-performance photodetectors based on suspended ultralong CNTs-MoS_2 heterojunction networks. Advanced Functional Materials, 2024: 2421980